Article No. jmbi.1999.3230 available online at http://www.idealibrary.com on IDEAL® J. Mol. Biol. (1999) 294, 223–237

JMB

Mutational and Structural Analysis of the Binding Interface between Type I Interferons and their Receptor Ifnar2

Jacob Piehler and Gideon Schreiber*

Department of Biological Chemistry, Weizmann Institute of Science, 76100, Rehovot Israel

Type I interferons (IFN) exert pleiotropic activities through binding to two cell surface receptors, ifnar1 and ifnar2. We are investigating the biophysical basis of IFN signaling by characterizing the complex of the extra-cellular domain of ifnar2 (ifnar2-EC) with IFNs on the level of purified recombinant proteins *in vitro*. Here, we present a detailed mutational study on the functional epitopes on both IFN and ifnar2. Kinetic and thermodynamic parameters were determined by label-free heterogeneous phase detection. On IFNα2, a relatively small functional epitope comprising ten amino acid residues was localized, which is nearly entirely formed by residues on the AB loop. Two hot-spot residues, L30 and R33, account for two-thirds of the total interaction energy. Comparing the anti-viral potency of the various mutants to the binding affinity towards ifnar2 revealed a proportional correlation between the two, suggesting a rate-limiting role of ifnar2 binding in IFN signaling. On ifnar2, residues T46, I47 and M48 were identified as hot-spots in the interaction with IFNα2. For another ten residues on ifnar2, significant contribution of interaction energy was determined. Based on these data, the functional epitope on ifnar2 was defined according to a homology model based on other members of the class II hCR family in good agreement with the complementary functional epitope on IFNα2. Although IFNα2 and IFNβ bind competitively to the same functional epitope, mutational analysis revealed distinct centers of binding for these IFNs on ifnar2. This small shift of the binding site may result in different angular orientation, which can be critically coupled to cytoplasmic signaling.

Keywords: type I interferon receptor; protein-protein interaction; kinetics; structure-function; mutational analysis

*Corresponding author

Introduction

Type I interferons (IFN) are a family of homologues cytokines which very potently elicit an anti-viral and anti-proliferative state in cells. These pleiotropic properties of type I IFNs have found considerable attention since their discovery more than 40 years ago (Isaacs & Lindenmann, 1957). During the last decade, some basic principles of interferon signaling pathway have been unveiled. All human type I IFNs (IFNα, β, ω and τ) bind to a cell surface receptor consisting of two trans-membrane proteins, ifnar1 (Uze *et al.*, 1990) and ifnar2 (Novick *et al.*, 1994). These receptor components associate upon binding to IFN (Cohen *et al.*, 1995), leading to phosphorylation by kinases associated to the cytoplasmic domains of ifnar1 (Tyk2) and ifnar2 (JAK1) (Uze *et al.*, 1995; Velasquez *et al.*, 1995). While ifnar2 binds IFNs with moderate affinity ($K_D \sim$ 2-10 nM for IFNα2), the intrinsic affinity of human ifnar1 to IFNs is low ($K_D >$ 100 nM), stabilizing the ternary complex by approximately 10 to 20-fold (Cohen *et al.*, 1995). Although signaling to all type I IFNs is mediated through this cell surface receptor, considerable differences in the response to different interferons have been observed (e.g. Rani *et al.*, 1996). Particularly IFNβ exerts specific functions which might be caused by

Abbreviations used: EC, extra-cellular; IFN, interferon; ifnar, type I IFN receptor; R, receptor; hC, helical cytokine; GH, growth hormone; TF, tissue factor; RIfS, reflectometric interference spectroscopy; VSV, vesicular stomatitis virus.

E-mail address of the corresponding author: bcges@wiccmail.weizmann.ac.il

0022-2836/99/460223–15 $30.00/0

differences in signal transduction at the receptor level (Abramowich *et al.*, 1994; Velasquez *et. al.*, 1995; Domanski *et al.*, 1998; Lewerenz *et al.*, 1998; Lu *et al.*, 1998). Several models for the unique interaction of IFNβ with the receptor have been proposed (Lewerenz *et al.*, 1998; Russell-Harde *et al.*, 1999).

Type I interferons belong to the class of helical cytokines (Sprang & Bazan, 1993) and are built by five helices. The structures of several type I IFNs have been solved, such as murine IFNβ (Senda *et al.*, 1992), human IFNα2 (Radhakrishnan *et al.*, 1996; Klaus *et al.*, 1997), human IFMβ (Karpusas *et al.*, 1997) and ovine IFNτ (Radhakrishnan *et al.*, 1998). Numerous mutational studies have revealed functional important residues on IFNs (Mitsui *et al.*, 1993; Runkel *et al.*, 1998), which can be ascribed to distinct functional epitopes for the interaction with ifnar1 and ifnar2 (Bandu *et al.*, 1994; Seto *et al.*, 1995; Uze *et al.*, 1995). Much less structural and functional data is available for the receptor proteins, which belong to the class II helical cytokine receptor (hCR) family (Bazan *et al.*, 1990; Uze *et al.*, 1995). Their homology to hCRs with known structure, e.g. TFR (Harlos *et al.*, 1994; Muller *et al.*, 1996), IFNγR (Walter *et al.*, 1995) and GHR (de Vos *et al.*, 1992), allows for modeling of the 3D structure with reasonable reliability. For GHR and IFNγR, the crystal structure of the complex of the receptor in its ligand is also available (de Vos *et al.*, 1992; Walter *et al.*, 1995). Based on these structures, models for the receptor and the complex with IFNs have been proposed (Seto *et al.*, 1995; Uze *et al.*, 1995) and several residues contributing to binding were identified (Lewerenz *et al.*, 1998).

Understanding the mechanisms of how distinct activity profiles are exerted by different type I IFN subtypes through the same cell surface receptor proteins ifnar1 and ifnar2 is a prerequisite for designing IFN-like drugs with specific activities. We believe that this requires detailed biophysical characterization of the formation of the complex of IFN with its receptor, which initiates the signaling cascade. We are investigating the interactions of IFNs with its receptors on the level of purified recombinant proteins to elucidate structure, thermodynamics and kinetics of the complex formation. Recently we have succeeded in refolding active extra-cellular part of ifnar2 (ifnar2-EC) expressed in *Escherichia coli* and we have purified it to homogeneity with yields of a few milligrams per liter of cell culture (Piehler & Schreiber, 1999). Moreover, we have established methods for studying thermodynamics and kinetic of the interaction of ifnar2-EC with IFNs. Here, we present a systematic mutational analysis of the binding interface between ifnar2 and IFNα2 to define the functional epitope on both proteins in quantitative terms. Protein-protein interactions were investigated by heterogeneous phase detection monitoring the binding kinetics in real time. By determining the contributions of a number of residues on both ifnar2-EC and IFNα2, we defined the binding interface of the ifnar2-IFNα2 complex on both proteins and we quantitatively mapped differences in binding of IFNα2 and IFNβ to ifnar2.

Results

Theoretical considerations

We have shown before, that the simple relation:

$$K_D = \frac{k_d}{k_a} \tag{1}$$

between rate constants of association k_a and dissociation k_d, and the equilibrium dissociation constant K_D is valid for the formation of the ifnar2-EC-IFNα2 complex (Piehler & Schreiber, 1999). The interaction between two proteins A and B is typically described by a three-state energy profile including an encounter complex A:B, and a transition state with increased free energy compared to the free and complexed proteins (Figure 1). These early states of interaction A:B and $AB^{\ddagger}$ are stabilized by long-range electrostatic forces (Schreiber & Fersht, 1996; Selzer & Schreiber, 1999), while the final complex AB is stabilized mainly by short-range interactions. The dissociation constant K_D describes the interaction energy of the complex as a difference of the free energy of the free proteins and the free energy of the final complex AB according to:

$$\Delta G^0_{K_D} = RT \ln K_D \tag{2}$$

Thus, changes in $\Delta G^0_{K_D}$ upon mutation:

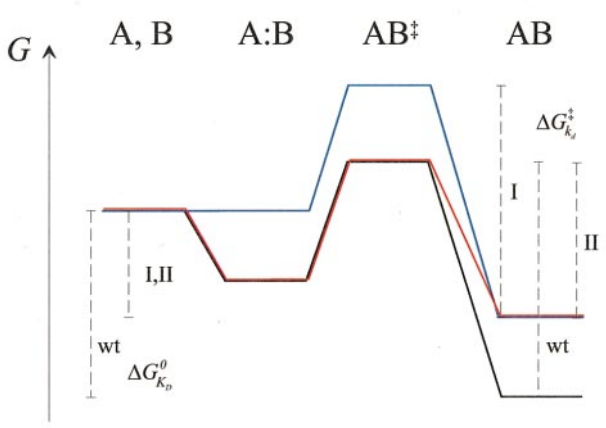

Figure 1. Free energy profiles for protein A and B forming a complex AB *via* an encounter complex A:B and a transition state $AB^{\ddagger}$. The profiles for two different types of mutations of the original proteins (black) are schematically depicted: mutation I (blue) exclusively removes long-range electrostatic forces, while mutation II (red) exclusively removes short-range forces. While these two mutated complexes have the same $\Delta G^0_{K_D}$, the difference in $\Delta G^{\ddagger}_{k_d}$ is considerable.

$$\Delta\Delta G^{0}_{K_D} = RT \ln \frac{K_D^{mut}}{K_D^{wt}} \quad (3)$$

identifies changes in both the long-range and short-range interactions. However, precisely defining residues in the binding interface requires discrimination of long and short-range interactions. According to transition-state theory, the kinetic rate constants describe the formation of the transition state. The rate of association has been shown to be affected mainly by the magnitude of long-range electrostatic forces between the proteins, which can be altered by mutations outside the binding site (Schreiber & Fersht, 1996; Selzer & Schreiber, 1999). Dissociation rates reflect the free energy $\Delta G^{\ddagger}_{k_d}$ required for breaking the short-range interactions in the binding site of the complex:

$$\Delta G^{\ddagger}_{k_d} = -RT \ln \frac{hk_d}{kT} \quad (4)$$

where k_d represents the dissociation rate constant. The change in $\Delta G^{\ddagger}_{k_d}$ upon mutation:

$$\Delta\Delta G^{\ddagger}_{k_d} = RT \ln \frac{k_d^{mut}}{k_d^{wt}} \quad (5)$$

is a much better measure for determining residues making short-range interactions than $\Delta\Delta G^{0}_{K_D}$, as it directly maps changes in the stability of the complex (cf. Figure 1). Measuring association and dissociation rate constants therefore allows for discriminating long and short-range forces contributing to affinity. Changes in the dissociation rate constant can also be determined with higher precision than changes in affinity because they are independent of the active protein concentration.

Rate constants of association and dissociation can be measured conveniently by label-free solid phase detection. Even though absolute values obtained by this method are often doubtful, relative parameters, such as $\Delta\Delta G$ values, have been determined to be very reliable (Cunningham & Wells, 1993; Albeck & Schreiber, 1999).

The ifnar2 binding site on IFNα2

The AB-loop and the D-helix have been identified before as being important for IFN activity (Mitsui *et al*., 1993) and are assumed to interact with ifnar2 (Seto *et al*. 1995; Uze *et al*., 1995). We mutated in IFNα2 most of the exposed residues from S25 to D35 on the AB-loop and from K121 to K134 on the D-helix to alanine, and determined the effect of mutation on the kinetics and thermodynamics of the interaction with ifnar2. All investigations were carried out with wild-type ifnar2-EC immobilized to the sensor surface, since rate constants and affinity determined by this configuration are self-consistent (Piehler & Schreiber, 1999). Typical binding curves for the interaction of wild-type IFNα2 and the mutant L26A are shown in Figure 2(a). Dissociation rate constants were determined at high protein concentrations to obtain a maximum amplitude. The dissociation curves for all IFNα2 mutants were fitted by a single exponential decay without systematic deviations. The dissociation rate constants were measured at least five times for each mutant, with typical standard deviations of less than 10 %. Association rate constants were determined under pseudo-first-order conditions at concentrations of 50 nM. Within the first 30 seconds, the association phase of the binding curve followed a single exponential function and was determined by direct fitting of a simple 1:1 kinetic model. Owing to the fast interaction kinetics and the additional parameters (concentration and the dissociation rate constant) the typical standard deviation of the association rate constants was ~20 %.

All kinetic and thermodynamic constants for the IFNα2 mutants binding to immobilized wild-type ifnar2-EC are summarized in Table 1. The association and the dissociation rate constants of the IFNα2 mutants in comparison to wild-type IFNα2 are shown in Figure 3. The precision of measurement allowed for the detection of down to ~20 % change in the dissociation rate constant (2σ criterion, $\alpha = 0.95$). A significant increase of the dissociation rate constant was found for the mutants L26A, F27A, L30A, K31A, D32A, R33A, H34A, D35A, R125A and K133A (Figure 3(b)). For the two mutants, R33A and L30A, the kinetics were too fast to be resolved by this method (>0.5 s^{-1}). A dissociation constant K_D of approximately 5 μM was found for the mutant L30A by titration on the surface (Figure 2(b) and (c)). Affinities determined by this method were shown to be consistent with the rate constants (Piehler & Schreiber, 1999). For the mutant R33A, no significant interaction with immobilized ifnar2-EC was detectable by this method up to concentrations of 50 μM of this mutant. Significant contributions of the association rate constant were observed for the three positively charged residues K31, K131 and K133 with the strongest contribution by K133. Since kinetic measurement allows for discrimination of long and short-range forces, the energetic contributions of the mutated residues to the stability of the complex were determined both from the dissociation rate constants ($\Delta\Delta G^{\ddagger}_{k_d}$) and from the affinity constant ($\Delta\Delta G^{0}_{K_D}$) (Table 1). The residues L30 and R33 are hot-spots on IFNα2, contributing approximately 15 kJ/mol and >15 kJ/mol, respectively. Except for residue L26, for which the energetic contribution is approximately 4 kJ/mol, all other residues investigated contribute less than 2 kJ/mol.

Anti-viral activity *versus* affinity of IFNα2 mutants

Binding of IFN to ifnar2 is the very first step initiating a complex signal transduction cascade which activates the anti-viral state in cells. Thus,

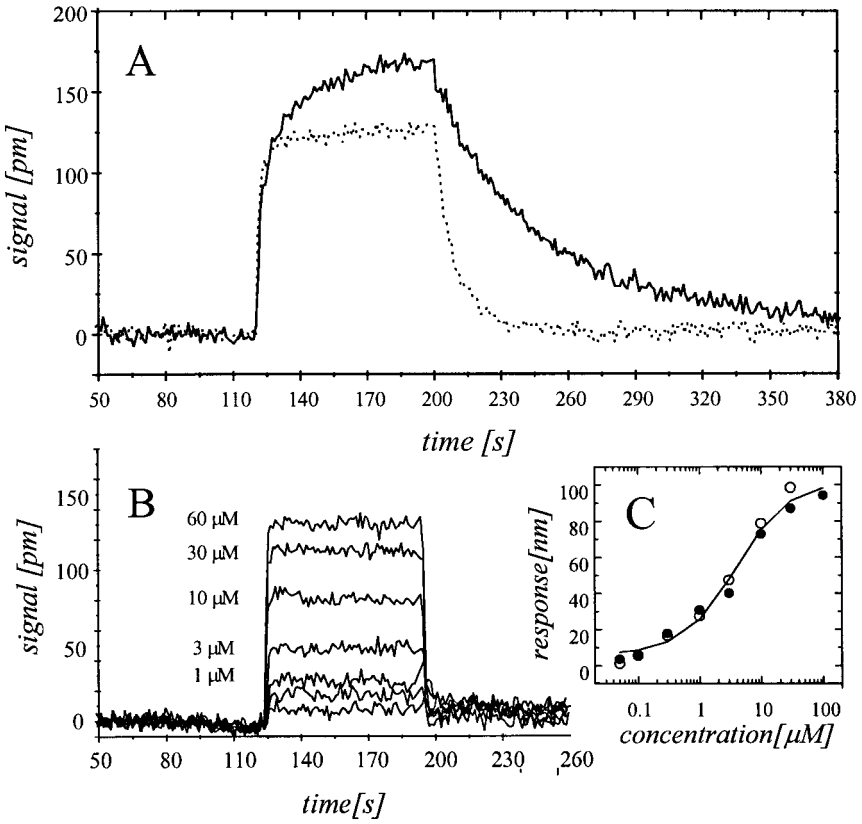

Figure 2. Measurement of kinetics and thermodynamics of the IFNα2 binding to immobilized wild-type ifnar2-EC by heterogeneous phase detection. (a) Association and dissociation of wild-type IFNα2 (500 nM, continuous line) and the mutant L26A (1.4 μM, broken line). (b) Binding curves for IFNα2 L30A at various concentrations. (c) Determination of K_D from a plot of the equilibrium response determined from B *versus* the concentration of L30A (two measurements for each concentration) according to Piehler & Schreiber (1999).

correlation between kinetics and thermodynamics of binding of different IFN mutants to ifnar2-EC and the relative potency of their antiviral response could define limiting steps in formation of the ternary complex required for signaling. The anti-viral activity of the IFNα2 mutants relative to wild-type IFNα2 were determined from the concentrations required to protect 50 % of human WISH cells challenged with vesicular stomatitis virus (VSV). We found that the relative activity of the mutants decreased proportional to the relative decrease in affinity determined by heterogeneous phase detection (Figure 4). Assuming that this correlation is also valid at lower activities, the affinity of the mutant R33A can be estimated from its relative anti-viral activity (of 6×10^5 units/mg) to be approximately 30 μM.

The binding site for IFNα2 on ifnar2

Three crystal structures of receptors from the hCR super-family with a similar topology as ifnar2-EC have been solved: TFR, IFNγR and GHR. While TFR has 21 % identity and 33 % similarity with ifnar2-EC, and IFNγR has 17 % identity and 33 % similarity, the homology of GHR to inar2-EC is significantly lower. Therefore, we used only the structures of TFR and IFNγR for homology modeling. The final alignment chosen for modeling is shown in Figure 5. Because of the rather low homology, the sequence alignment is ambiguous and different models are possible. The positioning of the gaps within the sequence of ifnar2 compared to the TFR sequence proved to be particularly critical. The sequence alignment of ifnar2 to IFNγR appeared more reliable: in the N-terminal domain where the binding site was mapped, only a single gap of two residues occurs, which location is defined by structural conserved regions. We therefore took the model based on IFNγR for all further structural considerations. A model of ifnar2-EC based on TFR as template with the alignment shown in Figure 5, however, gave a RMS deviation of all backbone atoms of 1.35 Å compared to the IFNγR based structure.

The region presumably involved in the interaction with IFN can be identified by comparison with the homologous systems GH/GHR and IFNγ/IFNγR, for which the structures of the complex have been solved (Seto *et al.*, 1995; Lewerenz *et al.*, 1998). Functional contributions of some residues in this region have already been confirmed by a mutational study on ifnar2 (Lewerenz *et al.*, 1998). To confine this binding site on ifnar2, we

Table 1. Thermodynamic and kinetic constants for the interactions of wild-type IFNα2 and several mutants with wild-type ifnar2-EC

IFNα2 mutant	k_a [a] (10^6 $M^{-1}s^{-1}$)	k_d [a] (s^{-1})	K_D [b] (nM)	$\Delta\Delta G^{\ddagger}_{k_d}$ [d] (kJ/mol)	$\Delta\Delta G^{0}_{K_D}$ [e] (kJ/mol)	Activity[f] (10^8 units/mg)
wt	2.1	0.020	10	-	-	4.0
S25A	2.1	0.015	7	−0.8 (0.2)	−0.8 (0.4)	n.d.
L26A	2.1	0.114	55	4.2 (0.2)	4.1 (0.4)	0.9
F27A	1.9	0.046	24	1.9 (0.1)	2.1 (0.3)	2.4
S28A	2.3	0.022	10	0.2 (0.2)	−0.0 (0.4)	n.d.
L30A	-	-	~5000[c]	-	~15	0.04
K31A	1.3	0.030	23	1.0 (0.2)	2.0 (0.3)	2.8
D32A	2.1	0.041	19	1.7 (0.2)	1.6 (0.4)	2.6
R33A	-	-	>5000[c]	-	>15	0.006
H34A	1.8	0.037	20	1.4 (0.2)	1.7 (0.4)	2.8
D35A	2.1	0.031	15	1.0 (0.1)	0.9 (0.4)	3.0
E41A	2.1	0.021	10	0.1 (0.1)	0.0 (0.5)	4.4
K121A	1.9	0.024	12	0.4 (0.2)	0.0 (0.4)	4.0
R125A	1.9	0.034	18	1.2 (0.2)	1.4 (0.4)	3.4
L128A	2.1	0.021	9	0.1 (0.3)	−0.2 (0.4)	5.1
K131A	1.4	0.023	16	0.3 (0.1)	1.2 (0.3)	3.0
E132A	2.4	0.019	8	−0.2 (0.1)	−0.5 (0.4)	3.8
K133A	0.9	0.033	37	1.1 (0.1)	3.2 (0.4)	1.3
K134A	1.8	0.021	11	0.1 (0.3)	0.3 (0.5)	n.d

[a] All rate constants were measured by heterogeneous phase detection with immobilized wild-type ifnar2-EC. The standard deviations from at least five independent measurements were $\sigma < 10\,\%$ for all k_d and $\sigma < 20\,\%$ for all k_a.
[b] Determined from the rate constants $K_D = k_d/k_a$ if not noted otherwise; $\sigma < 20\,\%$.
[c] Determined from equilibrium binding at the surface as shown in Figure 2(b) and (c); the standard error is ~25 %.
[d] Determined from k_d according to equation (3) (25 °C); σ is in parentheses.
[e] Determined from K_D according to equation (5) (25 °C); $\sigma < 20\,\%$.
[f] Anti-viral activity on human WISH cells with VSV as challenging virus relative to NIH IFNβ standard. The standard error from a fit of 16 data points was ~10 %.

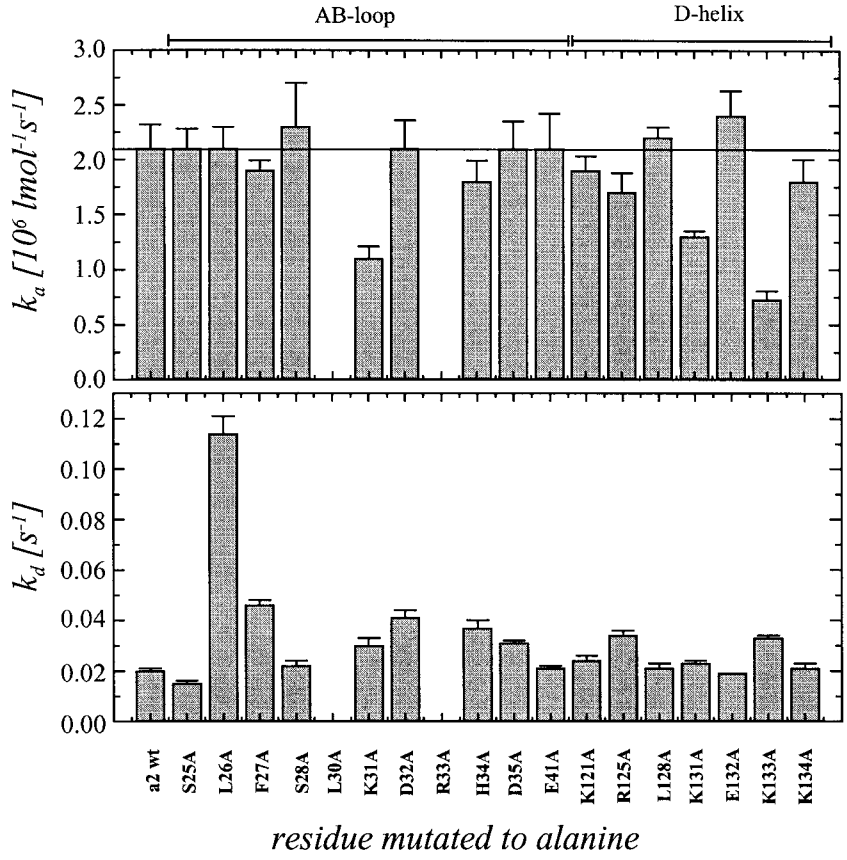

Figure 3. Comparison between the kinetic rate constants determined for the interaction of wild-type and mutant IFNα2 with immobilized wild-type ifnar2-EC (data from Table 1). Rates of L30A and R33A were too fast to be determined. Error bars indicate the standard deviations from at least five independent measurements.

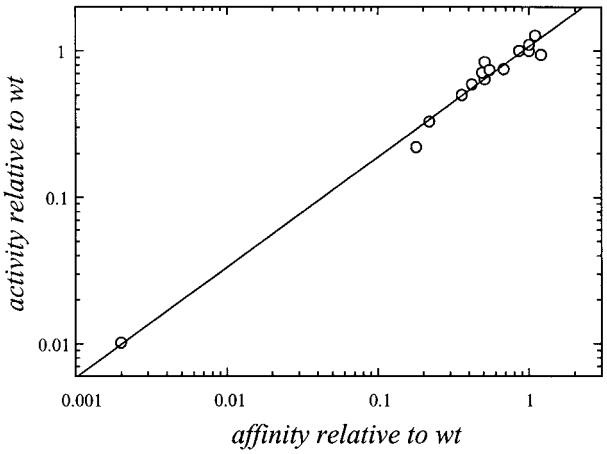

Figure 4. Correlation between the relative antiviral activity of different IFNα2 mutants with the relative affinity of the mutants determined by heterogeneous phase detection (data from Table 1).

probed long-range electrostatic interactions by a set of single charge reverse mutants: D8R, E30R, E52R, D72R, E86R, E134R, D140R and D191R. The effects on the dissociation kinetics was investigated by heterogeneous phase detection with IFNα2 wild-type being immobilized (Table 2). Based on these data, a number of residues in the binding site were individually mutated into alanine: T46, I47, M48, S49, K50, E52, D53, W74, S76, T77, H78, E79, N100, W102, I105, H189, D191 and E192. The dissociation kinetics of these mutants was compared to wild-type ifnar2-EC with immobilized IFNα2 (Figure 6(a)). In order to characterize the energetic contribution of residues towards binding more precisely, changes in kinetics and thermodynamics of the interaction with IFNα2 were investigated with the ifnar2-EC mutants being immobilized. Immobilization of ifnar2-EC mutants gave active surfaces for most mutants with typical R_{max} values between 100 and 300 pm (60-200 pg/mm^2) and a similar stability as the wild-type. For some mutants, however, no stable and active surfaces were obtained: the mutants E134R and W74A quickly lost their activity when immobilized on a surface, whereas W74F remained stable on the surface. For immobilized E79A, no binding activity could be measured for the immobilized protein indicating complete denaturation of this mutant by the immobilization procedure. The affinity of this mutant was estimated by a binding inhibition assay in solution. All the thermodynamic and kinetic data measured for the interaction of these mutants with wild-type IFNα2 are given in Table 2. Though the absolute dissociation rate constants are different for the ifnar2-EC mutants with either IFNα2 or ifnar2-EC immobilized, the relative change in the dissociation rate constant, and thus the $\Delta\Delta G^{\ddagger}_{kd}$, determined are in good agreement (Figure 6(b)). This result proves that these relative parameters are widely independent from experimental artifacts. A total of 14 out of the 24 mutated residues investigated significantly affected the interaction with IFNα2. The residue M48 was identified as a hot-spot for the binding of IFNα2, contributing more than 15 kJ/mol of binding energy. Mutations of T46 and I47 to Ala decrease binding by more than tenfold. E79 to Ala (but not to Gln) as well as I105 to Ala decreased the affinity to IFNα2 by four- to fivefold. The very low stability of the mutant E79A suggests that the residue E79 stabilizes not only the integrity of the binding site, but also seems to be important for the stability of the protein. A more precise characterization of the contribution of this residue towards binding of IFNα2 might be achieved by a more stable homologue mutant or by a different immobilization procedure. The mutations S49A, K50A, W74F, H78A and

```
ifnar2-EC   4    DSPDYTDES CTFKISLRNF RSILSWELKN HSIVPTHYTL LYTIMSKPED
TFR         1    SGTTNTVAA YNLTWKSTNF KTILEWEPKP V----NQVYT VQISTK---S
IFNgR       9   DLGPSSVPTP TNVTIESYNM NPIVYWEYQI MPQVPVFTVE VKNYGVKNSE

ifnar2-EC  54   LKVVKNCANT TRSFCDLTDE WR-STHEAYV TVLEGF---- -SG-NTTLFS
TFR        43   GDWKSKCFYT TDTECDLTDE IVKDVKQTYL ARVFSYPAGN VES-TEPLYE
IFNgR      59   --WIDACINI SHHYCNISDH VG-DPSNSLW VRVKAR---- -VGQKESAYA

ifnar2-EC  97   CSHNFWLAID MSFEPPEFEI VGFT-NHINV MVKFP----- ---------S
TFR        96   NSPEFTPYLE TNLGQPTIQS FEQVGTKVNV TVEDERTLVR RNNTFLSLRD
IFNgr     101   KSEEFAVCRD GKIGPPKLDI RKEEKQIMID IFHPSVFVNG DEQEVDYDPE

ifnar2-EC 132   IVEEELQFDL SLVIEEQSEG IVKKHKPEIK GNMSGNFTYI IDKLIPNTNY
TFR       146   VFGKDLIYTL YYWKSS---- -GKKTAKTNT ------NEFL IDVDK-GENY
IFNgr     151   TTCYIRVYNV YVRMNG-SEI QYKILTQKED DCDEIQCQLA IPVSSLNSQY

ifnar2-EC 182   CVSVYLEHS- --DEQAVIKS PLKCTLLPPG QESEFS
TFR       186   CFSVQAVIPS RTVNRKSTDS PVECMG---- ------
IFNgR     200   CVSAEGVLH- -VWGVTTEKS KEVCITIFNS SI----
```

Figure 5. Sequence alignment of ifnar2-EC to IFNγR and TFR used for homology modeling. Note that alignment of ifnar2 to IFNγR along the first fibronectin like domain (residues 1-105) is almost perfect, with only one short (two residue) gap.

Table 2. Thermodynamic and kinetic constants for the interaction of wild-type IFNα2 with wild-type and mutant ifnar2-EC

	IFNα2							IFNβ			
ifnar2-EC mutant	k_a [a] (10^6 $M^{-1}s^{-1}$)	k_d [a] (s^{-1})	k_d [b] (s^{-1})	K_D [c] (nM)	$\Delta\Delta G^{\ddagger}_{k_d}$ [f] (kJ/mol)	$\Delta\Delta G^{\ddagger}_{k_d}$ [g] (kJ/mol)	$\Delta\Delta G^{0}_{K_D}$ [h] (kJ/mol)	k_d (s^{-1})	K_D (nM)	$\Delta\Delta G^{\ddagger}_{k_d}$ [f] (kJ/mol)	$\Delta\Delta G^{0}_{K_D}$ [h] (kJ/mol)
wt	2.1	0.020	0.038	10	-	-	-	0.017	5[e]		-
D8R	-	-	0.034	-	-	−0.2 (0.2)	-	-	-	-	-
E30R	-	-	0.036	-	-	−0.1 (0.2)	-	-	-	-	-
T46A	-	0.189	-	130[d]	5.5 (0.3)	-	6.5 (0.5)	0.081	-	3.8 (0.4)	-
I47A	-	0.289	-	-	6.5 (0.3)	-		0.289	-	7.0 (0.3)	-
M48A	-	> 0.4	-	∼5000[d]	-	-	15.4 (0.6)	0.148	-	5.3 (0.3)	-
S49A	2.1	0.047	0.086	22	2.1 (0.2)	2.0 (0.2)	2.1 (0.4)	0.071	-	3.5 (0.3)	-
K50A	2.6	0.053	0.125	17	2.3 (0.2)	3.0 (0.3)	1.9 (0.5)	0.019	-	0.3 (0.3)	-
E52R	1.3	0.040	0.053	30	1.6 (0.2)	0.9 (0.2)	2.8 (0.5)	0.026	-	1.0 (0.3)	-
E52A	2.2	0.032	0.046	14	1.1 (0.3)	0.5 (0.2)	1.0 (0.5)	-	-		-
D53A	-	-	0.033	-	-	−0.3 (0.3)	-	-	-		-
K55A	1.8	0.034	0.098	19	1.3 (0.2)	2.2 (0.4)	1.7 (0.4)	0.025	-	0.9 (0.2)	-
D72R	-	-	0.035	-	-	−0.2 (0.3)	-	-	-		-
W74A	-	-	0.116	-	-	2.8 (0.3)	-	-	-		-
W74F	1.6	0.055	0.113	34	2.5 (0.2)	2.7 (0.4)	3.2 (0.6)	0.022	-	0.7 (0.5)	-
S76A	2.0	0.033	0.081	17	1.2 (0.2)	1.9 (0.2)	1.4 (0.3)	0.017	-	−0.1 (0.6)	-
T77A	-	0.021	0.035	-	0.1 (0.1)	−0.2 (0.3)		0.021	-	0.5 (0.3)	-
H78A	1.9	0.055	0.120	29	2.5 (0.1)	2.9 (0.2)	2.7 (0.4)		-	−1.9 (0.6)	-
E79A	-	-	-	∼50[e]	-	-	∼4	-	∼10[e]		1.7
E86R	-	-	0.042	-	-	0.3 (0.2)	-	-	-	-	-
N100A	2.2	0.016	0.033	7	−0.6 (0.2)	−0.3 (0.2)	−0.7 (0.4)	0.005	-	−3.1 (0.5)	-
W102A	1.8	0.063	0.111	35	2.7 (0.1)	2.7 (0.3)	2.9 (0.5)	-	∼500[d]	-	11.0
I105A	-	0.107	-	-	4.1 (0.3)	-	-	0.093	-	4.2 (0.3)	-
E134R	-	-	0.033	-	0.0 (0.1)	−0.3 (0.3)	-	-	-	-	-
D140R	1.8	0.017	0.026	9	−0.5 (0.1)	−0.9 (0.3)	0.1 (0.4)	0.020	-	0.5 (0.2)	-
H189A	-	0.024	0.054	-	0.4 (0.2)	0.9 (0.3)	-	-	-	-	-
D191R	1.5	0.034	0.061	23	1.3 (0.2)	1.2 (0.2)	2.1 (0.5)	-	-	-	-
D191A	2.2	0.017	0.040	8	−0.4 (0.3)	0.2 (0.2)	−0.4 (0.4)	0.022	-	0.7 (0.4)	-
E192A	2.1	0.030	0.051	13	0.7 (0.2)	0.8 (0.2)	0.7 (0.3)	0.014	-	−0.5 (0.5)	-

[a] Measured by heterogeneous phase detection with wild-type and mutant ifnar2-EC being immobilized. The standard deviations (σ) from at least five independent measurements were <10 % for all k_d with IFNα2, <25 % for all k_d with IFNβ and <20 % for all k_a.
[b] Measured by heterogeneous phase detection with wild-type IFNα2 immobilized, σ < 10 %.
[c] Determined from the rate constants $K_D = k_d/k_a$, σ < 20 %.
[d] Determined from equilibrium binding at the surface, σ ∼ 20 %.
[e] Estimated from binding inhibition assay in solution as described before (Piehler & Schreiber, 1999), σ ∼25 %.
[f] $\Delta\Delta G^{\ddagger}_{k_d}$ determined from k_d (ifnar2-EC immobilized) according to equation (5) (25 °C), with σ in parentheses.
[g] $\Delta\Delta G^{\ddagger}_{k_d}$ determined from k_d (IFNα2 immobilized) according to equation (5) (25 °C), with σ in parentheses.
[h] $\Delta\Delta G^{K_D}$ determined from K_D according to equation (3)(25 °C), with σ in parentheses.

W102A each increased the dissociation rate constant between two- and threefold compared to wild-type ifnar2. The mutants E52A, K55A and S76A increased the dissociation rate constant by less than twofold, suggesting that these residues are positioned in the periphery of the binding site. For all other alanine mutants, dissociation rate constants similar to wild-type ifnar2-EC were observed. Significant changes in the association rate constant were observed for the charge reverse mutants E52R and D191R (decreased k_a), as well as for K50A (increased k_a), indicating that a negative field on ifnar2 is required for electrostatic steering.

Comparison of IFNα2 and IFNβ binding to ifnar2-EC

Accurate measurement of the interaction kinetics of single alanine mutations in the binding site of ifnar2 allowed mapping of differences in binding of IFNα2 and IFNβ. Strong non-specific binding interfered with studying the interaction of immobilized ifnar2-EC with IFNβ under physiological ionic strength. Increasing the salt concentration up to 500 mM eliminated the non-specific binding to the transducer surface. Therefore, all investigations involving IFNβ were carried out under these conditions. The dissociation rate constant of IFNα2 decreased by 10 % at this salt concentration compared to 150 mM, but still single-phase kinetics were observed. The maximum response by IFNβ was approximately 10-20 % higher than that of IFNα2, in agreement with the higher molecular mass of the glycosylated, CHO-produced IFNβ. The first 70 % of the dissociation amplitude were fitted by a single exponential decay, with a rate constant of 0.017 s^{-1} for immobilized wild-type ifnar2-EC. Binding curves for IFNα2 and IFNβ are shown in Figure 7 in comparison for two different ifnar2-EC mutants. The association kinetics of IFNβ significantly deviated from a simple single exponential model and was not further evaluated.

The changes in interaction energy of mutants of ifnar2-EC ($\Delta\Delta G^{\ddagger}_{k_d}$ if available, otherwise $\Delta\Delta G^{\ddagger}_{K_D}$, cf. Table 2) for wild-type IFNα2 and IFNβ are compared in Figure 8. Most residues of

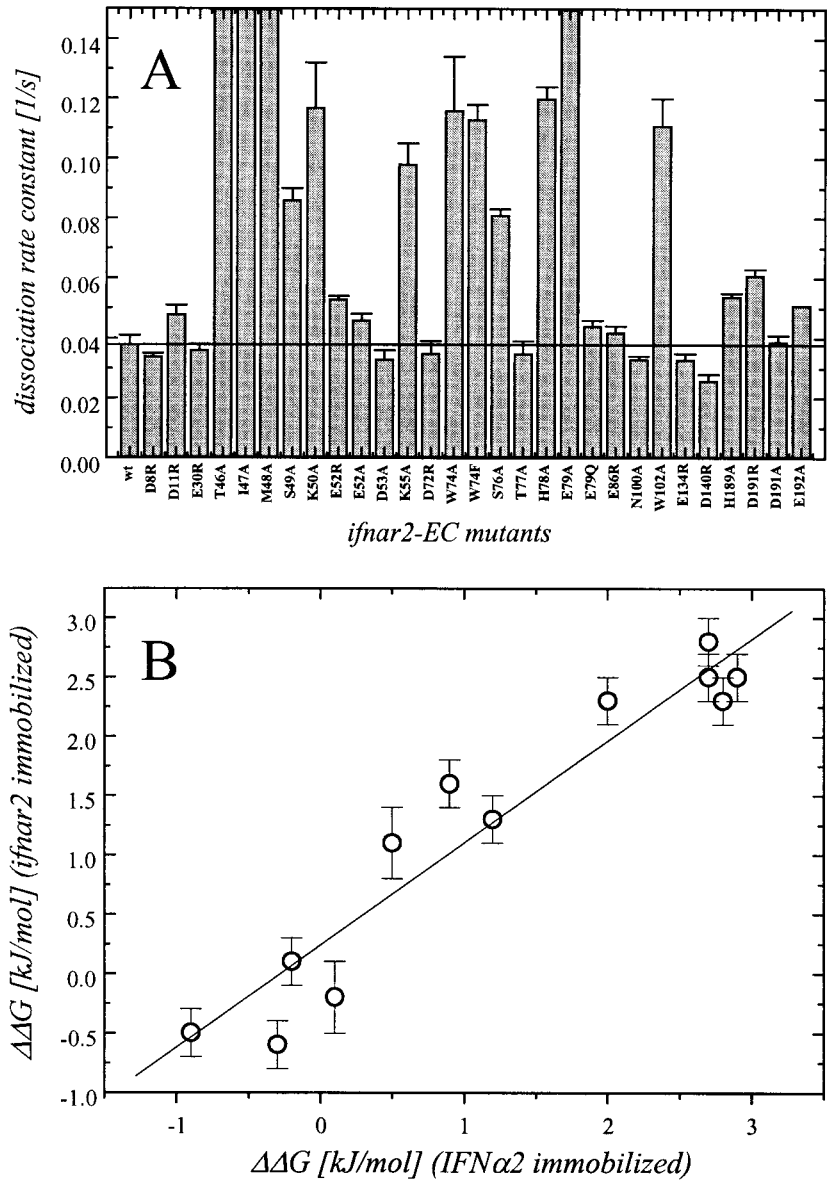

Figure 6. Characterization of ifnar2-EC mutants. (a) Dissociation rate constants measured with wild-type IFNα2 immobilized to the surface. (b) Comparison of $\Delta\Delta G^{\ddagger}_{k_d}$ obtained from measurements with immobilized IFNα2 and ifnar2-EC, respectively. Data are from Table 2.

ifnar2-EC that are destabilizing the complex with IFNα2, also affect the binding of IFNβ. However, the relative energetic contributions to binding of IFNα2 and IFNβ are very different for most residues. The mutation W102A results in a tenfold stronger decrease in affinity to IFNβ compared to IFNα2. The mutation M48A, which destabilizes the complex with IFNα2 by about 500-fold, decreased the affinity towards IFNβ only eightfold. Furthermore, the mutant H78A stabilizes the complex with IFNβ nearly twofold, while destabilizing the complex with IFNα2 more than twofold. The mutation N100A hardly affects the rates for binding IFNα2, whereas its decreasing the dissociation rate constant for IFNβ by almost fourfold (cf. the binding curves in Figure 7). For the residues K50, E52 and W74F, no significant changes in affinity to IFNβ were found upon mutation, while they significantly contributed to binding of IFNα2 with ifnar2-EC.

Discussion

Understanding the activity profiles exerted by different type I IFNs requires a thermodynamic, kinetic and structural understanding of the recognition by the cell surface receptor. As a first step towards this goal, we have carried out a rigorous mutational analysis of the binding interface of the complex formed between ifnar2 and type I IFNs. The energetic contributions of amino acid residues were mapped in a quantitative manner using purified proteins for measuring affinity and kinetics of the complex formation. Heterogeneous phase detection was used for precise comparison of the rate constants and the affinity of different IFNs and its mutants. A principal problem of mutational

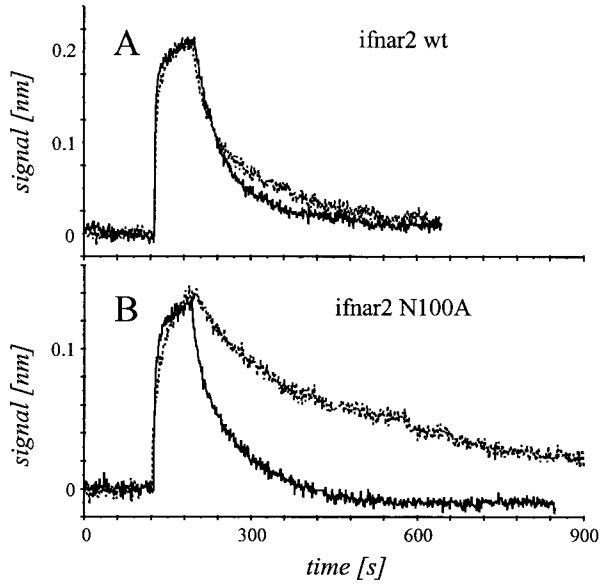

Figure 7. Comparison of the binding curves for wild-type IFNα2 (—) and IFNβ (· · · · · ·) with immobilized (a) wild-type ifnar2-EC and (b) the mutant N100A.

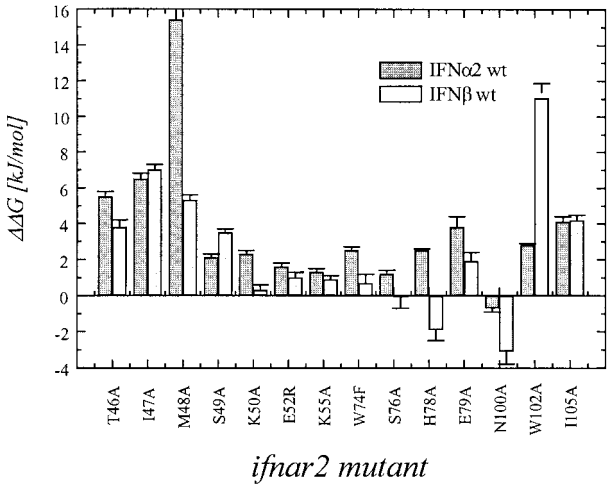

Figure 8. Comparison of the energetic contributions of residues in the binding site of ifnar2 to binding of IFNα2 and IFNβ (data from Table 2).

analysis of a binding site is to discriminate between mutations which affect its structural integrity, from mutations which specifically remove interactions in the interface. In case of IFNα2, the importance of residues for the structural integrity of the binding site can be estimated from the structure, and only exposed residues in the vicinity of the hot-spot of binding were analyzed. The case is more difficult for ifnar2, because small shifts in sequence alignment can exchange exposed and buried residues. Some mutations on ifnar2-EC affected the stability of the protein (e.g. Y81A, W74A), indicating an effect on the structure of ifnar2. According to our model structure, these two residues are buried within the core of ifnar2. Thus, the stability of the ifnar2 mutants gave at least an estimate of whether residues are exposed or buried. All charge-reverse mutations which are located outside the binding site (D8R, E30R, D72R, E86R, E134R and D140R) did not significantly affect the interaction, suggesting that in general mutations on the surface of ifnar2 affect binding only when they are located at the vicinity of the binding site. This is true even for the extreme case of charge-reverse mutants. Furthermore, very different effects upon mutation on the interaction with IFNα2 and IFNβ were observed. This was most pronounced for the mutants M48A and W102A which are hot-spots of binding for IFNα2 and IFNβ, respectively. These mutants apparently affect the binding very locally, excluding considerable effects on the structural integrity of the entire binding site.

Until now, all mutational studies of the binding site on IFNα2 have been based on the assessment of pleiotropic activities of chimaric or point-mutated IFNs (reviewed by Mitsui *et al.*, 1993). We found a good correlation of the anti-viral activity of IFNα2 mutants with their affinity toward ifnar2-EC, which confirms the principal validity of conclusion drawn from activity assays. The residues on IFNα2 which contribute to the interaction with ifnar2 are in good agreement with residues identified previously by measuring changes in antiviral activity (Camble *et al.*, 1986; Tymms *et al.*, 1989; Waine *et al.*, 1992; Wang *et al.*, 1994). Assessment of the kinetics and thermodynamics of IFN binding to ifnar2 enables us to characterize its role in IFN signaling. The correlation between affinity and activity of IFN is striking. This correlation holds true not only for the IFNα2 mutants we investigated here. Our thermodynamic and kinetic data for ifnar2-EC mutants also correlate with anti-viral activities of IFNs measured on cells with mutated ifnar2 (Lewerenz *et al.*, 1998). In particular, differences in anti-viral activity of IFNα2 and IFNβ observed with cells with the ifnar2 mutants M48A and W102A correlate with the differences we found in the affinity. The apparently linear downstream propagation (tyrosine phosphorylation and formation of the transcription factor ISGF3) of these effects shown in the same study corroborates the central role of the affinity of IFNs to ifnar2 for function. Such correlation is not trivial, since the formation of a ternary complex by at least two consecutive binding events is required for signal transduction. In the case of the structural homologous and functionally similar GH-GHR system, the affinity of GH to its receptor surpasses the requirements for activity by about 30-fold, and any further increase in affinity by decreasing k_d did not decrease the EC_{50} dose (Pearce *et al.*, 1999). The limiting step in formation of the ternary GH complex is probably the association of GH to the first receptor (binding to site 1), while the long half-life

of this complex (~one hour) is longer than is required to ensure the formation of a ternary complex within a single binding event. For GH mutants with dissociation rate constants higher than ~0.016 s^{-1}, a linear correlation between affinity and activity has been observed (Pearce *et al.*, 1999). The half-life of the binary complex of <one minute is probably too short to guarantee the formation of a productive ternary complex within a single binding event. In this case, equilibrium occupancy of the receptor (k_a *versus* k_d) determines the probability of the formation of the ternary complex. This situation corresponds to the IFNα2-receptor system with a k_d of 0.02 s^{-1}, which is strikingly close to the critical k_d in the GH system. Though the critical k_d, below which no further increase in activity can be achieved, has yet to be verified for the binding of IFNs, increasing the activity of IFNs should be possible by increasing k_a.

The total free energy of the IFNα2-ifnar2-EC complex ΔG^0 is approximately 54 kJ/mol at room temperature assuming the unitary standard state of 55 M given by the concentration of water molecules. Interaction energies $\Delta\Delta G^0_{K_D}$ determined from single point mutations are not strictly additive, because cooperative effects are not taken into account. Furthermore, interactions with the backbone and C^β atoms are not mapped by alanine scanning analysis. However, the sum of $\Delta\Delta G^0_{K_D}$ for individual mutations gives an estimation as to what extent the binding site is mapped by the residues investigated (Cunningham & Wells, 1993). For IFNα2, the sum of the interaction energies $\Delta\Delta G_{K_D}$ of all residues investigated is approximately 53 kJ/mol, which is close to the free energy of the complex formation. This agreement suggests that the functional epitope is essentially built from the residues we have identified. Further contributions to the total complex free energy have to be ascribed to long-range electrostatic interactions, which considerably increase the basal association rate constant (~5 kJ/mol at physiological ionic strength; Piehler & Schreiber, 1999). The two residues L30 and R33 on IFNα2 account for nearly two-thirds of ΔG^0, together with L26 and F27 for more than 75 % of ΔG^0. The functional epitope on IFNα2 for binding to ifnar2 according to these considerations is depicted by the solution structure of IFNα2 (Klaus *et al.*, 1997) shown in Figure 9. The key residues L30 and R33 (colored in red in Figure 9) are close to each other and form together with L26 and F27 a hydrophobic patch on IFNα2 (and probably other IFNα, which have a highly conserved sequence in this region). This region contributes the dominant part of the interaction energy and can be assumed as the very center of the binding site. Six residues adjacent to this patch also show significant interaction with ifnar2; however, none of them decreases the complex stability (as measured by the change in k_d) by more than twofold (orange colored residues in Figure 9). These six residues are all charged, suggesting that they predominantly interact by electrostatic forces. Except for R125 and K133, which are both in the periphery of the binding site, all residues contributing to binding of ifnar2 are localized on the AB-loop (Figure 9(b)). Thus, peptides analogous to the AB-loop might mimic the binding site of IFNα2, providing a potential lead structure for designing low molecular mass antagonists.

A quantitative determination of the rate constant of the complex formation allows for discriminating of long and short-range forces contributed by specific residues. We have shown before that long-range electrostatic forces considerably enhance the

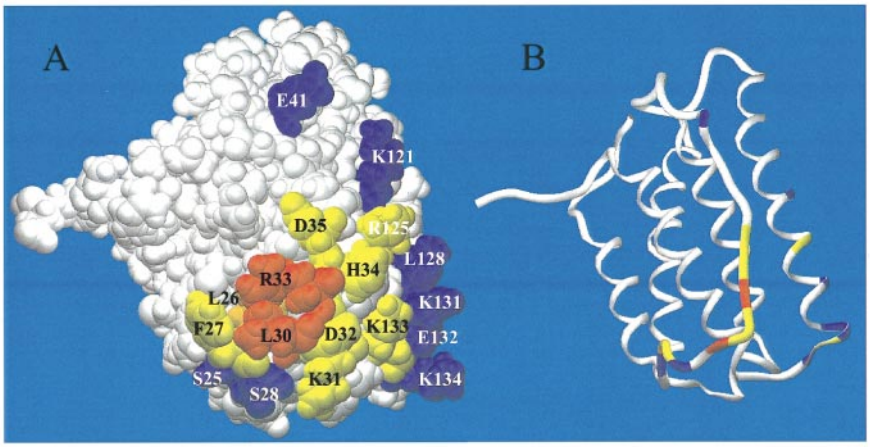

Figure 9. The functional epitope for binding ifnar2 on IFNα2 (solution structure of IFNα2 according to Klaus *et al.* (1997)). (a) Space-filling representation; (b) ribbon model including the side-chains of the mutated residues. The hot-spot residues R33 and L30 are colored red, L26 is colored orange and the other residues with significant effect on complex stability (F27, K31, D32, H34, D35, R125, K133) are colored yellow. Indifferent residues (S25, S28, K121, L128, E132 and K134) and residue K131, which contributes exclusively by long-range forces, are depicted in blue. This picture was composed with the Swiss-PDB Viewer (Guex & Peitsch, 1997).

association of the IFNα2-ifnar2-EC complex (Piehler & Schreiber, 1999). In agreement with the theory of electrostatic rate enhancement, only mutations of charged residues (K31, K131 and K133) on IFNα2 affected the association rate constant. Mutation of these positive residues into neutral residues decreased k_a, indicating that the positive electric field in the periphery of the functional epitope is important for steering the association with ifnar2. This observation supports our notion that a binding site is preferably mapped using $\Delta\Delta G^{\ddagger}_{k_d}$ as a criterion for allocating a residue in the binding site.

In comparison to the functional epitope of GH for the interaction with GHR (de Vos *et al.*, 1992; Cunningham & Wells, 1993), the number of contact residues on IFNα2 is much smaller, suggesting a significant smaller buried surface of the complex with ifnar2. This observation matches the differences observed in binding kinetics of the two complexes. Both association and dissociation rate constants of binding of GH to its receptor (3×10^5 M^{-1} s^{-1} and 2.7×10^{-4} s^{-1}, respectively, for binding of GH site 1; Cunningham & Wells, 1993) are much smaller than for IFNα2-ifnar2. The lower association rate constants indicates less long-range electrostatic forces involved in the GH-GHR interaction, while the lower dissociation rate constant indicates more stabilizing contacts in the interface.

We have characterized the functional epitope on ifnar2 for the binding of IFNα2 and IFNβ. A number of residues on ifnar2 were identified which contributed to binding both IFNα2 and IFNβ. The binding sites resulting for IFNα2 and IFNβ from these investigations are depicted on our homology model of ifnar2-EC (Figure 10). The key residue on ifnar2 for binding of IFNα2 is M48. Mutating this residue to Ala reduces binding by 500-fold (15 kJ/mol). Two additional residues located nearby (T46 and I47) reduce binding by over tenfold (5.5 and 6.5 kJ/mol, respectively). These three relative hydrophobic hot-spot residues are surounded by six, mostly polar residues (S49, K50, H78 E79, W102 and I105) which contribute between 2 and 4 kJ/mol binding energy. Residue W74 in our model is buried beneath this binding site. This is in agreement with the low stability of ifnar2-EC observed for the alanine mutant of W74 (which was not observed for the phenylalanine mutant) and the considerable decrease of complex stability upon mutation. In agreement with previous investigations (Lewerenz *et al.*, 1998), our results indicate hardly any contact of IFNα2/IFNβ with the C-terminal domain of ifnar2, which is considerably involved in the homologous complex of GH and IFNγ with their receptors (de Vos *et al.*, 1992;

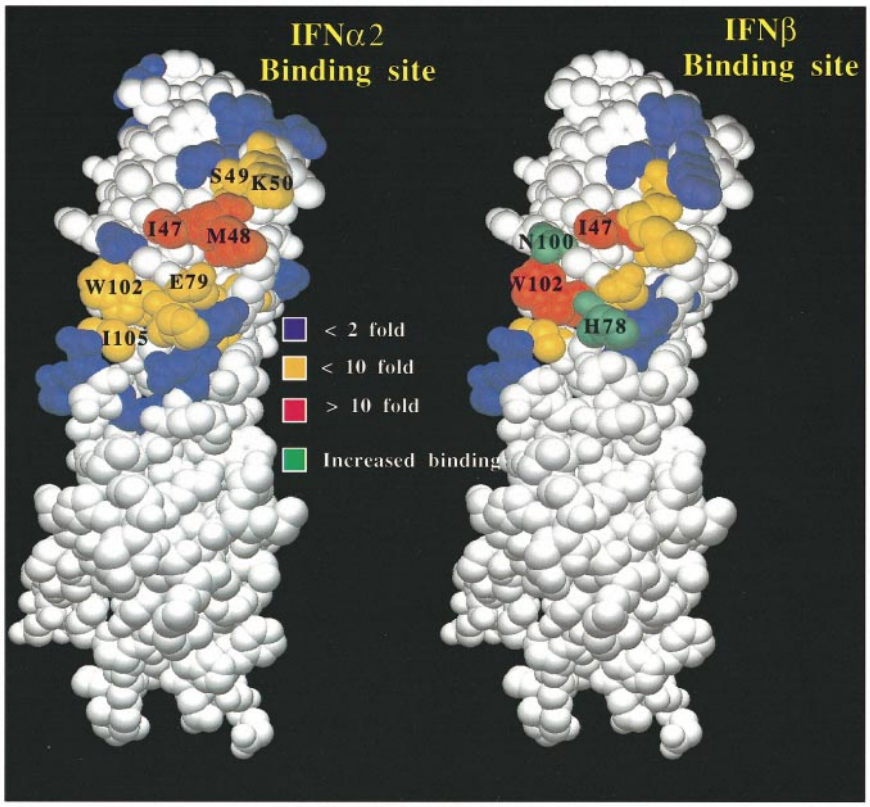

Figure 10. Comparison of the functional epitope of ifnar2 for IFNα2 and IFNβ (homology model of ifnar2-EC with IFNγR as template). The residues are color-coded according to their contribution to binding IFNα2 or IFNβ as indicated in the Figure. This picture was composed with the Swiss-PDB Viewer (Guex & Peitsch, 1997).

Clackson *et al.*, 1998; Walter *et al.*, 1995). Some contribution of residue E192 was found and none for the residues E134, D140, H189 and D191. However, this perfectly agrees with the small functional epitope identified on IFNα2 and the binding site on ifnar2 fits very well to its binding site on IFNα2. The key residues M48 and I47 form a hydrophobic patch which could interact with the hydrophobic patch on IFNα2 (F27 and L30). For ifnar2-EC, patches of negatively charged residues at the periphery of the binding site (E52/D53, E134-E137 and D191/E192) contribute to steering of association through long-range attraction of the positive residues in the periphery of the functional epitope of IFNα2, driving the fast rate of association of this complex. It is interesting to note that all the residues on ifnar2 identified by us to be important in binding are located on loops and not beta-sheets. A similar distribution of binding residues has been observed for the interaction of GH with GH-R, and on antibodies. The sum of the interaction energies for all residues involved in binding IFNα2 identified so far accounts for 52 kJ/mol, which is close to the total interaction energy of the complex.

Dissecting the binding epitope of IFNβ on ifnar2 shows a similar location of the binding site, but with a very different distribution of binding energies of specific residues. The most important residues on ifnar2 binding IFNβ are W102 (11 kJ/mol) and I47 (7 kJ/mol). Other residues important for binding include T46, M48, S49 and I105 (3-5 kJ/mol). Two mutations on ifnar2 (H78 and N100) result in an decreased rate of dissociation (and thus a higher affinity) for IFNβ but not for IFNα2. It would be interesting to explore the phenotype of a H78, N100 double mutation in ifnar2, which should have about 20-fold tighter binding for IFNβ compared to IFNα2. Overall, much lower effect of the mutations investigated on the binding of IFNβ was observed. The sum of the interaction energies is 39 kJ/mol for IFNβ, which is approximately two-thirds of the total interaction energy (~57 kJ/mol). Further residues of the functional epitope on ifnar2 interacting with IFNβ have yet to be identified.

Structural differences have been proposed to be responsible for different activity profiles of different IFNs, especially IFNα2 and IFNβ (Domanski *et al.*, 1998; Lewerenz *et al.*, 1998; Russell-Harde *et al.*, 1999). Comparing the contributions of different residues located on ifnar2 to the binding of IFNα2 and IFNβ, allows mapping such differences in a quantitative manner. Our results suggest that IFNα2 and IFNβ essentially bind to the same binding site on ifnar2 with very similar kinetic and thermodynamic parameters. Albeit the contributions of specific residues to binding are significantly different. Comparing the functional epitope of IFNα2 and IFNβ on ifnar2 (Figure 10) suggests that despite the overlapping binding site, the angular orientation of both ligands binding ifnar2 may differ. This could lead to a different orientation of the intra-cellular domains of ifnar2 and ifnar1 in the ternary complex, which could be critical in the pattern of activation of the cellular response to IFNα2 *versus* IFNβ. This fact is in good agreement with mutational studies of the binding site on IFNβ (Runkel *et al.*, 1998). Mutation of the residue R35 of IFNβ resulted in a much less dramatic loss in activity than the homologous mutation of R33 on IFNα2. Despite the considerable sequence homology between IFNα2 and IFNβ in the AB-loop, the spatial arrangement of the residues most important for binding is quite different (Figure 11). The overall structural deviation in the homologue sequence C29-R33 (C31-R35 on IFNβ) is 1.75 Å, while for the residues L26 and F27, which play a considerable role in forming the functional epitope on IFNα2, no homology on IFNβ is observed. The fact that a loop structured so differently binds to essentially the same epitope on ifnar2 might indicate structural changes upon binding.

With the quantitative, high-resolution description of the functional epitopes on IFNα2 and ifnar2, and the correlation of thermodynamics with activity, we have made an important step towards an understanding of IFN recognition by its receptor on a molecular level. We were able to prove the importance of the affinity of IFNα2 toward ifnar2 for their activity, which may account for the varying potency of different IFNs. Although IFNα2 and IFNβ bind competitive to the same functional epitope, mutational analysis revealed distinct centers of binding for these IFNs on ifnar2. In the ternary complex IFN-ifnar1-ifnar2, small shifts of the binding site may result in different angular orientation, which can be critically coupled to cytoplasmic signaling as been shown for another hCR (Livnah *et al.*, 1998).

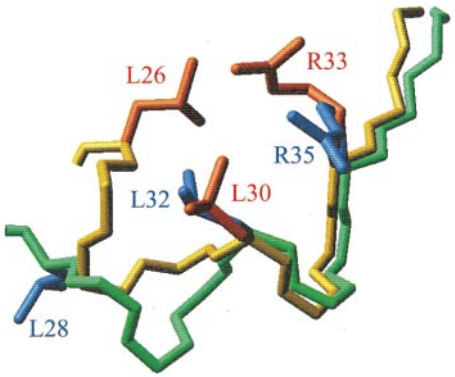

Figure 11. The backbone of the AB-loop from L26 to D35 for IFNα2 (orange) and L28 to D37 for IFNβ (green), with the most important residues on IFNα2, L26, L30 and R33 in red and the corresponding residues on IFNβ (L28, L32 and R35) in blue. This picture was composed with the Swiss-PDB Viewer (Guex & Peitsch, 1997).

Materials and Methods

Protein expression and purification

IFNα2 and ifnar2-EC were expressed in *E. coli* and were purified by ion-exchange and size-exclusion chromatography as described (Piehler & Schreiber, 1999). The levels of expression of IFNα2 and ifnar2-EC mutants were as high as the wild-type. The fraction of successfully refolded IFNα2 mutants varied, with typical yields between 10 and 50 mg protein per liter of cell culture, purified to over 95% homogeneity. The IFNα2 mutants Y129A and R120A gave very low yields of active protein (<1 mg/l cell culture). These mutants were not further investigated. Significantly lower yields of properly refolded ifnar2-EC (approximately 20% compared to the wild-type) were obtained for the mutants W74A, E79A and E134R. However, the mutant W74F again gave yields similar to the wild-type. Y81A did not give active protein. Wild-type, glycosylated IFNβ produced in CHO cells was a gift from Professor M. Rubinstein. Protein concentrations were determined from the absorbance at 280 nm (Piehler & Schreiber, 1999) with $\varepsilon_{280} = 18{,}070\ M^{-1}$ for IFNα2, $\varepsilon_{280} = 30{,}050\ M^{-1}$ for IFNβ and $\varepsilon_{280} = 26{,}500\ M^{-1}$ for ifnar2-EC (corrected to $\varepsilon_{280} = 21{,}100\ M^{-1}$ for the tryptophan mutants of ifnar2-EC W102A and W74F). Protein purity was analyzed by SDS-PAGE under non-reducing conditions and concentrations were verified by quantitative evaluation of the protein bands compared to wild-type standard. Concentrations of active IFNα2 protein were determined by analytical gel filtration with ifnar2-EC as described (Piehler & Schreiber, 1999).

Site-directed mutagenesis

Site-directed mutagenesis was carried out by PCR of the plasmids for expression (pT72Cα2 and pT72CR2) with 18-21 nucleotide primers containing the mutated codon using high fidelity polymerases *pwo* (Boehringer Mannheim) and *Pfu* (Stratagene) as described in detail (Albeck & Schreiber, 1999). After phosphorylation and ligation, the mutated plasmids were transformed into TG1 cells. The sequence of the whole expressed gene containing the mutation was verified by DNA sequencing.

Thermodynamic and kinetic analysis

All thermodynamic and kinetic data were obtained from label-free heterogeneous phase detection. The interaction between IFNα2 and ifnar2-EC was monitored by reflectometric interference spectroscopy (RIfS) under flow-through conditions as described (Piehler & Schreiber, 1999). Either ifnar2-EC (wild-type or mutant) or wild-type IFNα2 was immobilized by standard amide coupling chemistry. All measurements with IFNα2 and ifnar2-EC were carried out in 50 mM Hepes with 150 mM NaCl and 0.01% Triton X100 at pH 7.4. The interaction with IFNβ was measured at 500 mM NaCl in order to eliminate non-specific interactions with the surface, which was observed at 150 mM NaCl.

Association and dissociation kinetics were measured by standard injection protocols and corrected by blank runs. Dissociation rate constants were measured at protein concentration of 0.5-2 μM in order to saturate the surface. The total range of dissociation was used for fitting a 1:1 kinetic model. Association rate constants were determined by incubating IFNα2 (wild-type and mutants) at a concentration c of 50 nM under pseudo-first-order conditions. Consistency of the observed rate constants at different concentrations with a single association rate constant under these conditions has been shown before (Piehler & Schreiber, 1999). The first 30 seconds of the binding curve $R(t)$ was fitted by a 1:1 kinetic model:

$$R(t) = R_{eq}(1 - e^{-(k_a c + k_d)t}) \quad (6)$$

(R_{eq}, equilibrium response) using the mean dissociation rate constant determined in previous experiments. All rate constants were determined as mean values from at least five independent measurements and the errors are given by their standard deviations σ. Differences between two mean values of more than 2σ were considered significant ($\alpha = 0.95$). For fast dissociating mutants, dissociation constants K_D were determined from the equilibrium binding on the surface at different concentrations as described before (Piehler & Schreiber, 1999). For signal correction, the immobilized ifnar2-EC was denatured and the background response was measured at the same concentrations. Equilibrium dissociation constants in solution were determined by a binding inhibition assay with immobilized ifnar2-EC as described (Piehler & Schreiber, 1999).

Anti-viral protection activity assay

Anti-viral activity of wild-type and mutant IFNα2 was assayed as the inhibition of the cytopathic effect of VSV on human WISH cells (Rubinstein *et al.*, 1981). The activity of wild-type and mutant IFNα2 was determined from the relative concentration needed for 50% protection of the cells compared to NIH IFNβ standard. The dissociation constant K_D of IFNβ binding to wild-type ifnar2-EC was determined by a binding inhibition assay as described (Piehler & Schreiber, 1999).

Homology modeling of ifnar2-EC

A structural model of the extracellular part of the ifnar2 (212 amino acid residues) from SYDSP (N-ter) to ESEFS (C-ter) (Novick *et al.*, 1994) was built using homology modeling. Sequence alignment was carried out using Ψ-BLAST and clustalX (with ten different homologous protein sequences), taking into account the secondary structure motifs in TFR and IFNγR. The alignment was corrected manually by moving gaps from β-sheets into loops. Homology modeling was done using Swiss-PDBViewer 3.0 and the automated comparative protein modeling server SWISS-MODEL in optimized mode (Guex & Peitsch, 1997). As primary template for modeling we used the structure of IFNγR.

Acknowledgments

We thank M. Rubinstein and D. Novick for supplying IFNβ and for many helpful discussions, S. Barak for performing numerous IFN cytopathic activity assays, and S. Albeck for the critical reading of the manuscript. This work was supported by grant no. 96-00439/1 from the US-Israel Binational Science Foundation (BSF). J.P. is an EMBO postdoctoral fellow, 1998-1999.

References

Abramovich, C., Shulman, L. M., Ratovistski, E., Harroch, S., Tovey, M. G., Eid, P. & Revel, M. (1994). Differential tyrosine phosphorilation of the IFNAR chain of the type I interferon receptor and an associated surface protein in response to IFNα and IFNβ. *EMBO J.* **13**, 5871-5877.

Albeck, S. & Schreiber, G. (1999). Biophysical characterization of the interaction of the β-lactamase TEM-1 with its protein inhibitor BLIP. *Biochemistry,* **38**, 11-21.

Bandu, M.-T., Horisberger, M. A., Dorques, A., Lutfalla, G. & Mogensen, K. E. (1994). Domains of interaction between alpha interferon and its receptor components. *J. Mol. Biol.* **243**, 245-257.

Bazan, J. F. (1990). Structural design and molecular evolution of a cytokine receptor superfamily. *Proc. Natl Acad. Sci. USA,* **87**, 6934-6938.

Camble, R., Petter, N. N., Trueman, P., Newton, C. R., Carr, F. J., Hockney, R. C., Moore, V. E., Greene, A. R., Holland, D. & Edge, M. D. (1986). Functionally important conserved amino-acids in interferon-alpha 2 identified with analogues produced from synthetic genes. *Biochem. Biophys. Res. Commun.* **134**, 1404-1411.

Clackson, T., Ultsch, M. H., Wells, J. A. & deVos, A. M. (1998). Structural and functional analysis of the 1:1 growth hormone:receptor complex reveals the molecular basis for receptor affinity. *J. Mol. Biol.* **277**, 1111-1128.

Cohen, B., Novick, D., Barak, S. & Rubinstein, M. (1995). Ligand-induced association of the type I interferon receptor components. *Mol. Cell. Biol.* **15**, 4208-4214.

Cunningham, B. C. & Wells, J. A. (1993). Comparison of a structural and a functional epitope. *J. Mol. Biol.* **234**, 554-563.

de Vos, A. M., Ultsch, M. & Kossiakoff, A. A. (1992). Human growth hormone and extracellular domain of its receptor: crystal structure of the complex. *Science,* **255**, 306-312.

Domanski, P., Nadeau, O. W., Platanias, L. C., Fish, E., Kellum, M., Pitha, P. & Colamonici, O. R. (1998). Differential use of the betaL subunit of the type I interferon receptor determines signaling specificity for IFN α2 and IFN β. *J. Biol. Chem.* **273**, 3144-3147.

Guex, N. & Peitsch, M. C. (1997). SWISS-MODEL and the Swiss-PdbViewer: an environment for comparative protein modeling. *Electrophoresis,* **18**, 2714-2723.

Harlos, K., Martin, D. M. A., O'Brien, D. P., Jones, E. Y., Stuart, D. I., Polikarpov, I., Miller, A., Tuddenham, E. G. D. & Boys, C. W. G. (1994). Crystal structure of the extracellular region of human tissue factor. *Nature,* **370**, 662-666.

Isaacs, A. & Lindenmann, J. (1957). Virus interference I: the interferon. *Proc. Roy. Soc. London ser. B,* **147**, 258-267.

Karpusas, M., Nolte, M., Benton, C. B., Meier, W., Lipscomb, W. N. & Goelz, S. (1997). The crystal structure of human inteferon β at 2.2 Å resolution. *Proc. Natl Acad. Sci. USA,* **94**, 11813-11818.

Klaus, W., Gsell, B., Labhardt, A. M., Wipf, B. & Senn, H. (1997). The three-dimensional high resolution structure of human interferon alpha-2a determined by heteronuclear NMR spectroscopy in solution. *J. Mol. Biol.* **274**, 661-675.

Lewerenz, M., Mogensen, K. E. & Uze, G. (1998). Shared receptor components but distinct complexes for alpha and beta interferons. *J. Mol. Biol.* **282**, 585-599.

Livnah, O., Johnson, D. L., Stura, E. A., Farrell, F. X., Barbone, F. P., You, Y., Liu, K. D., Goldsmith, M. A., He, W., Krause, C. D., Pestka, S., Jolliffe, L. K. & Wilson, I. A. (1998). An antagonist peptide EPO receptor complex suggests that receptor dimerization is not sufficient for activation. *Nature Struct. Biol.* **5**, 993-1004.

Lu, J., Chuntharapai, A., Beck, J., Bass, S., Ow, A., De Vos, A. M., Gibbs, V. & Kim, K. J. (1998). Structure-function study of the extracellular domain of the human IFN-α receptor (hIFNAR1) using blocking monoclonal antibodies: the role of domains 1 and 2. *J. Immunol.* **160**, 1782-1788.

Mitsui, Y., Senda, T., Shimazu, T., Matsuda, S. & Utsumi, J. (1993). Structural, functional and evolutionary implications of the three-dimensional crystal structure of murine interferon beta. *Pharmac. Ther.* **58**, 93-132.

Muller, Y. A., Ultsch, M. H. & de Vos, A. M. (1996). The crystal structure of the extracellular domain of human tissue factor refined to 1.7 A resolution. *J. Mol. Biol.* **256**, 144-159.

Novick, D., Cohen, B. & Rubinstein, M. (1994). The human interferon alpha/beta receptor: characterization and molecular cloning. *Cell,* **77**, 391-400.

Pearce, K. H., Jr, Cunningham, B. C., Fuh, G., Teeri, T. & Wells, J. A. (1999). Growth hormone binding affinity for its receptor surpasses the requirements for cellular activity. *Biochemistry,* **38**, 81-89.

Piehler, J. & Schreiber, G. (1999). Biophysical analysis of the interaction of human ifnar2 expressed in *E. coli* with IFNα2. *J. Mol. Biol.* **289**, 57-67.

Radhakrishnan, R., Walter, L. J., Hruza, A., Reichert, P., Trotta, P. P., Nagabhushan, T. L. & Walter, M. R. (1996). Zinc mediated dimer of human interferon-alpha 2b revealed by X-ray crystallography. *Structure,* **4**, 1453-1463.

Radhakrishnan, R., Walter, L. J., Subramaniam, P. S., Johnson, H. M. & Walter, M. R. (1998). Crystal structure of ovine interferon-t at 2.1 Å resolution. *J. Mol. Biol.* **286**, 151-162.

Rani, S. M. R., Foster, G. R., Leung, S., Leaman, D., Stark, G. R. & Ransohoff, R. M. (1996). Characterization of beta-R1, a gene that is selectively induced by interferon-beta (IFN-beta) compared with IFN-alpha. *J. Biol. Chem.* **271**, 22878-22884.

Rubinstein, S., Familletti, P. C. & Pestka, S. (1981). Convenient assay for interferons. *J. Virol.* **37**, 755-758.

Runkel, L., Pfeffer, L., Lewerenz, M., Monneron, D., Yang, C. H., Murti, A., Pellegrini, S., Goelz, S., Uze, G. & Mogensen, K. (1998). Differences in activity between alpha and beta type I interferons explored by mutational analysis. *J. Biol. Chem.* **273**, 8003-8008.

Russell-Harde, D., Wagner, T. C., Perez, H. D. & Croze, E. (1999). Formation of a uniquely stable type I interferon receptor complex by interferon β dependent upon particular interactions between IFNβ and its receptor and independent of tyrosine phophorylation. *Biochem. Biophys Res. Commun.* **255**, 539-544.

Schreiber, G. & Fersht, A. R. (1996). Rapid, electrostatic assisted, association of proteins. *Nature Struct. Biol.* **3**, 427-431.

Selzer, Z. & Schreiber, G. (1999). Predicting the rate enhancement of protein complex formation from the electrostatic energy of interaction. *J. Mol. Biol.* **287**, 409-419.

Senda, T., Shimazu, T., Matsuda, S., Kawano, G., Shimizu, H., Nakamura, K. T. & Mitsui, Y. (1992).

Three-dimensional crystal structure of recombinant murine interferon-beta. *EMBO J.* **11**, 3193-3201.

Seto, M. H., Harkins, R. N., Adler, M., Whitlow, M., Church, W. B. & Croze, E. (1995). Homology model of human interferon-alpha8 and its receptor complex. *Protein Sci.* **4**, 655-670.

Sprang, S. R. & Bazan, J. F. (1993). Cytokine structural taxonomy and mechanisms of receptor engagement. *Curr. Opin. Struct. Biol.* **3**, 815-827.

Tymms, M. J., McInnes, B., Waine, G. J., Cheetham, B. F. & Linnane, A. W. (1989). Functional significance of amino acid residues within conserved hydrophilic regions in human interferons-alpha. *Antiviral Res.* **12**, 37-47.

Uze, G., Lutfalla, G. & Gresser, I. (1990). Genetic transfer of a functional human interferon α receptor into mouse cells: Cloning and expression of its cDNA. *Cell,* **60**, 225-234.

Uze, G., Lutfalla, G. & Mogensen, K. E. (1995). α and β interferons and their receptor and their friends and relations. *J. Interferon Res.* **15**, 3-26.

Velazquez, L., Mogensen, K. E., Barbieri, G., Fellous, M., Uze?, G. & Pellegrini, S. (1995). Distinct domains of the tyrosine kinase Tyk2 required for high affinity binding of alpha/beta IFNs and for signal transduction. *J. Biol. Chem.* **270**, 3327-3334.

Waine, G. J., Tymms, M. J., Brandt, E. R., Cheetham, F. & Linnane, A. W. (1992). Structure-function study of the region encompassing residues 26-40 of human interferon α4: Identification of residues for antiviral and anti-proliferative activities. *J. Interferon Cytokine Res.* **12**, 43-48.

Walter, M. R., Windsor, W. T., Nagabhushan, T. L., Lundell, D. J., Lunn, C. A., Zauodny, P. J. Z. & Narula, S. K. (1995). Crystal structure of a complex between interferon-gamma and its soluble high-affinity receptor. *Nature,* **376**, 230-235.

Wang, L., Hertzog, P. J., Galanis, M., Overall, M. L., Waine, G. J. & Linnane, A. W. (1994). Structure-function analysis of human IFN-alpha. Mapping of a conformational epitope by homologue scanning. *J. Immunol.* **152**, 705-715.

Edited by J. A. Wells

(Received 9 July 1999; received in revised form 28 September 1999; accepted 28 September 1999)